Computers and Fluids, Vol.117, pp. 11-16 (2015) DOI: 10.1016/j.compfluid.2015.04.024

Thermodynamic properties of phase separation in shear flow

R.S. Qin*

Department of Engineering & Innovation, the Open University, Walton Hall, Milton Keynes MK7 6AA, United Kingdom

Abstract

The steady state thermodynamic properties of a binary-phase shear fluid are studied quantitatively using the compressible lattice Boltzmann BGK theory with mesoscopic inter-particle potentials. For the Newtonian van der Waals fluid, numerical calculation shows that the effect of boundary shear on steady state phase diagram of immiscible phases is negligible when the fluid is not in the near-critical region. Streamlines show no penetration of macroscopic flow through the interface to cause the mass density shift even when the boundary shear velocities are significant. The deformation of the droplets depends on the shear rate and interfacial energy but the change of phase diagram during deformation is negligible. In the near critical region, however, shear causes significant derivation in the phase diagram.

Keywords: Phase separation; Phase equilibrium; Lattice Boltzmann equation; Mesoscopic interparticle potentials

* Corresponding author: E-mail addresses: rongshan.qin@open.ac.uk. Tel: +44 1908 652 999; Fax: +44 1908 653 858.

I. Introduction

There are two methods to calculate the phase diagram of multiphase materials. One takes the system free energy as a starting point and minimizes its value to get the equilibrium thermodynamic information. Most commercial thermodynamic code packages (e.g. Thermo_Calc and MTDATA) are based on such approximation [1]. Another starts from the microscopic interactions and calculates the relationship between the materials structure and thermodynamic properties, where equilibrium is a state of dynamic balance. Molecular dynamics and *ab* initio are examples of this method [2]. For phase separation in shear flow, however, both methods encounter difficulty. On the one hand the free energy for multiphase fluid under shear is lacked and hence is impossible to use the free energy minimization method. Hydrodynamics and thermodynamics affect each other, e.g. shear enhances mass transfer but mass transfer is affected by the thermodynamic equilibrium. On the other hand a system showing macroscopic hydrodynamic effect is too big to be calculated using the microscopic interaction method. In this consideration, meso-scale model is introduced to bridge the gap between micro-scale and macro-scale computations. This allows studying the systems where both thermodynamics and hydrodynamics are equally important [3]. Many mesoscale models are based on mesoscopic interparticle potential. There are two methods to derive mesoscopic interparticle potential. One is called top-down method where the parameters in the mesoscopic interparticle potential ansatz are specified according to the macroscopic properties [3, 4]. Another is called bottom-up method where mesoscopic interparticle potentials are obtained by coarse-grained microscopic interactions [5, 6]. The aim of the present work is to use a recent developed mesoscopic interparticle potential to study the

phase equilibrium property of immiscible materials where phase separation takes place in shear flow [4].

Phase separation in shear flow has attracted considerable interest for years due to its wide application in industry [7]. For examples, shear-induced demixing is expected to improve the oil extraction where large amount of water is mixed with crude oil, and shear-induced mixing is thought to be able to produce aluminum-lead alloys which are implemented to make wear parts in automation industry. There are significant reports in literature on the experimental observations of both shear-induced mixing and shear-induced de-mixing [8, 9]. However, the question of whether the shear flow induces mixing or demixing inside a phase is still a subject of debate. Theoretical models on the effect of interactive force on the phase separation are mainly based on the kinetics such as internal degrees of freedom [10, 11]. The fundamental understanding of the phenomena is still at its early stage. The situation in same to the electric-field-induced phase separation, i.e., whether an electric field can induce mixing or demixing is still unsolved [12, 13]. This work aims to improve the understanding of the effect of shear on the steady state phase diagram.

To the purpose of the present work, the lattice Boltzmann (LB) model has been implemented to study the phase diagram of van der Waals shear flow. LB model is a special kind of particle-based computational technique in which particles are only allowed to move from one lattice to another without falling in between. The earliest LB model was constructed by McNamara and Zanetti [14]. The spirit of LB model is to describe fluid by mapping the fluid properties onto discrete lattices, while the physical

state and properties at each grid are described by a set of particle distribution functions $\{f_i(r, t)\}$. The macroscopic fluid variables, for example the density and velocity, are defined via moments of distribution function. The evolution of the system toward its equilibrium is through the relaxation of a particle distribution function to its equilibrium form $\{f_i^{eq}(r, t)\}$ [15]. The equilibrium particle distribution function was originally constructed artificially but has been put into a mathematically accurate scheme [16]. LB model has now achieved a state of sophisticate and has been used in tackling many problems successfully [17, 18]. The mesoscopic interparticle potential that possesses short-range strong Enskog repulsive and long-range weak mean field attractive interactions has been proved to be able to produce LB kinetic theory that is consistent with thermodynamics [19]. For the van der Waals fluids, a meso-scale interparticle potential has been derived and applied to reproduce the accurate equilibrium phase diagram, convincing interface property and irreversible thermodynamics [4]. It is possible to use the method to simulate the phase separation in shear flow and to examine the steady state thermodynamic properties quantitatively.

II. Modelling and theory

For a van der Waals fluid whose kinetic viscosity is η (viscosity per density) and mass density distribution is $\rho(r, t)$, fluid is confined in a pair of parallel shear boundaries in a distance of h and the top boundary moves toward right with a speed $v\vec{x}$ and the bottom boundary moves toward left with a speed $-v\vec{x}$, as illustrated in Fig. 1. The shear rate is given by $\dot{\gamma} = 2v/h$. The fluid is Newtonian and hence the kinetic viscosity is independent

of the mass density. The material is assumed to be isothermal. The temperature is denoted by T. The free energy of the system when $\dot{\gamma} = 0$ is represented by [20]

$$G(t) = \int \left\{ \frac{\varepsilon}{2} |\nabla \rho(\vec{r}, t)|^2 + g[\rho(\vec{r}, t), T] \right\} dr \tag{1}$$

where ε is the gradient parameter. It has been derived from thermodynamic and mathematic approximations that ε can be expressed as $\varepsilon = \sqrt{\partial^2 g[\rho, T] / \partial (\nabla \rho)^2 - 2\partial (\partial g[\rho, T] / \partial \nabla^2 \rho) / \partial \rho}$ [21]. It is obviously that ε is dependent of temperature T. $g[\rho(\vec{r}, t), T]$ is the free energy density at position *r* and time *t* of the bulk phase which takes following expression for van der Waals fluid [22]

$$g[\rho(\vec{r}, t), T] = \rho(\vec{r}, t) RT \ln\left(\frac{\rho(\vec{r}, t)}{1 - \rho(\vec{r}, t) b} \right) - a\rho(\vec{r}, t)^2 \tag{2}$$

where *a* and *b* are factors to represent the attraction between molecules and repulsion due to volume respectively. Phase separation follows the routine of $\delta G(t) / \delta t \le 0$ until the equilibrium. Eq. (2) can be used to calculate equilibrium phase diagram directly using the free energy minimization method. However, it cannot be used to calculate the steady state phase diagram when $\dot{\gamma} \neq 0$ because no shear effect is included in Eq. (2). The equation of state of van der Walls fluid at $\dot{\gamma} \neq 0$ can be derived from [18]

$$p = \rho \frac{\partial g[\rho, T]}{\partial \rho} - g[\rho, T] \tag{3}$$

where *p* is the pressure which takes the format of

$$p = \rho \frac{RT}{1 - \rho b} - a\rho^2 \tag{4}$$

The equation of state is used to determine the mesoscopic interparticle potentials. The interaction potential between point $\vec{r}$ and $\vec{r}'$ is defined as [17]

$$V(\vec{r},\vec{r}') = \wp\, w(\vec{r},\vec{r}')\psi(\vec{r})\psi(\vec{r}') \tag{5}$$

where $\wp$ is a signal function. $w(\vec{r},\vec{r}')$ is the weight factor that depends on the relative position between r and r'. $\psi(\vec{r})$ is derived based on the unification of equations of state and has [4]

$$\wp\,\psi(r)^2 = \frac{2b\rho(r)^2}{1-\rho(r)b} - \frac{2a\rho(r)^2}{RT} \tag{6}$$

where $\wp = -1$ when the right hand side of Eq. (6) is negative, or $\wp = 1$ vice versa.

In LB simulation of microstructure evolution, time flows is represented by the iteration of a series discrete time steps. Each time step contains three processes. The first is called propagation where particles migrate to their neighbor sites without falling in between. The second is called collision where each particle distribution function relaxes toward the equilibrium. The LB Bhatnagar-Gross-Krook (BGK) approximation defines a collision operator as following

$$f_i(\vec{r}+\hat{e}_i\Delta t, t+\Delta t) - f_i(\vec{r},t) = -\frac{1}{\tau}\left[f_i(\vec{r},t) - f_i^{eq}(\vec{r},t)\right] \tag{7}$$

where f_i is the instant particle distribution functions. $\vec{e}_i$ is the elementary speed vector as illustrated in Fig. 1. Δt is the time step. τ is the relaxation time which is related to kinetic viscosity of the fluid η by $\eta = (\tau\Delta t - 0.5)/3$. f_i^{eq} is called the equilibrium particle distribution function or equilibria. For the two dimensional nine velocity (i=0, 1, … 8) LB model (named D2Q9), f_i^{eq} takes format of following for compressible fluids [16]

$$f_i^{eq} = \rho w_i\left[1 + 3(\hat{e}_i\cdot\vec{u}) + 4.5(\hat{e}_i\cdot\vec{u})^2 - 1.5\vec{u}^{\,2}\right] \tag{8}$$

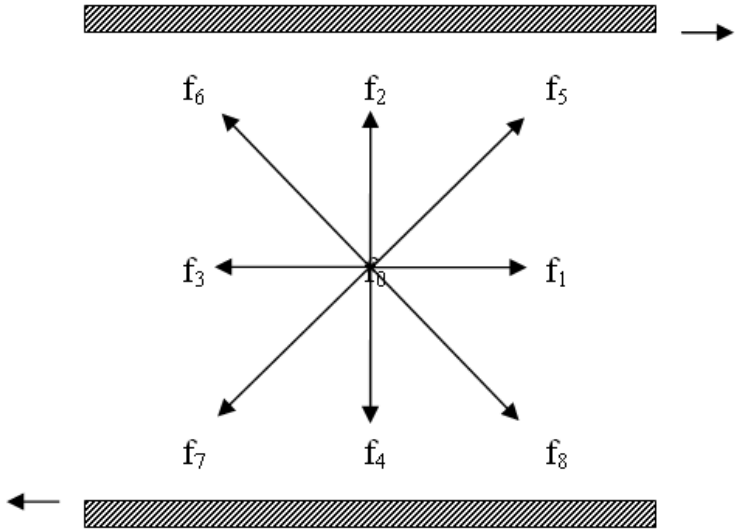


Fig. 1 Schematic diagram of shear boundaries and elementary speed vectors of D2Q9 lattice Boltzmann model

where the mass density is obtained from $\rho(\vec{r},t)=\sum_{i=0}^{8} f_i^{eq}(\vec{r},t)$. w_i is the weight factor and has $w_0=4/9$, $w_i=1/9$ for i=1,2,3,4 and $w_i=1/36$ for i=5,6,7,8. w_i in Eq. (8) and $w(\vec{r},\vec{r}')$ in Eq. (5) are the same. $\vec{u}(\vec{r},t)$ is the speed of lattice and its value is calculated via $\vec{u}(\vec{r},t)=\sum_{i=0}^{8} f_i^{eq}(\vec{r},t)\hat{e}_i/\rho(\vec{r},t)$. The expression of f_i^{eq} for incompressible liquid is different from Eq. (8) [23]. Multiplying Eq. (8) by 1 and summing over sub index *i* will lead to continuum equation, and multiply Eq. (8) by $\vec{e}_i$ and summing over sub index *i* leads to Navier-Stokes equation. The third process is called acceleration where the lattice speed $\vec{u}(\vec{r},t)$ is changed into $\vec{u}'(\vec{r},t)$ according to momentum conservation.

$$[\vec{u}'(\vec{r},t)-\vec{u}(\vec{r},t)]\rho(\vec{r},t)=-\tau\nabla\left[\sum_{r'\neq r}V(r,r')\right] \tag{9}$$

The particle distribution functions at shear boundaries are determined by the method given by Zou and He [24]. The method was based on the idea of bounceback of the non-equilibrium part. For those lattices located on the bottom boundary where the boundary is moving with speed $u_x\hat{x}+u_y\hat{y}$, the mass density and the unknown particle distribution functions are given by

$$\rho=\frac{1}{1-u_y}\left[f_0+f_1+f_3+2\left(f_4+f_7+f_8\right)\right] \tag{10.1}$$

$$f_2=f_4+\frac{2}{3}\rho u_y \tag{10.2}$$

$$f_5=f_7-\frac{1}{2}\left(f_1-f_3\right)+\frac{1}{2}\rho u_x+\frac{1}{6}\rho u_y \tag{10.3}$$

$$f_6=f_8+\frac{1}{2}\left(f_1-f_3\right)-\frac{1}{2}\rho u_x+\frac{1}{6}\rho u_y \tag{10.4}$$

where f_0 is obtained from the previous step. f_1, f_3, f_4, f_7 and f_8 are transferred into the site from the neighbor grids in propagation process. The unknown particle distribution on the lattice of top boundary can be obtained by rotating Eq. (10) with 180°. It is necessary to point out that Eq. (10) does not contain any capillary effect. The boundary condition was developed in order to generate correct shear velocity at boundary for single phase fluid. It is still an open question whether Eq. (10) will affect the wetting angle for multiphase fluid. Periodic boundary conditions are used for left and right boundaries.

III. Numerical simulations and discussions

Noise is introduced during the calculation of mesoscopic interactions by adding a small fluctuation to the mass density as following

$$\psi(\rho(\vec{r},t)) \to \psi\left(\sum_i f_i(\vec{r},t) + \mu\xi\right) \tag{11}$$

where μ is called fluctuation intensity and $\mu = 0.005$ is used in the simulations, ξ is a random number between –1 and 1. Mass conservation is maintained because no fluctuation is added to the mass density itself. There are two reasons for adding fluctuation in the simulation: (a) Each grid in LB represents a mesoscopic sub-system that contains thousands of molecules. The physical quantities in the grid are in statistical average. A fluctuation should be added to reflect the statistical nature. (b) A fluctuation helps to avoid the numerical trap in metatable state in order to achieve the global minimum free energy state. $\tau = 1$ is assumed in all the simulations because it can always be achieved by justifying the time step according to $\eta = (\tau\Delta t - 0.5)/3$. When the time step is defined, lattice distance Δx can be calculated by $\Delta x = c\Delta t$ where $c = \sqrt{3RT/m}$ is the lattice speed of sound and *m* is the molar weight of materials. The lattice numbers for a system of $L_x \times L_y$ are $L_x/\Delta x$ and $L_y/\Delta x$. The real dimension of the system is not important in the current work because the properties that are interested here are the steady state phase diagrams. The energy is defined in the unit of RT_c. The reduced temperature is implemented in the present work.

The van der Waals fluid with a = 1.018226 and b = 0.3 is considered. The parameters *a* and *b* are practically different for different type of materials. In this calculation, b=0.3 is chosen arbitrarily. a = 1.018226 is then chosen manually to allow the critical temperature for phase separation approaching to 1 for the convenience of numerical calculations. A proper method should be developed to convert all the parameters to dimensionless variables in the calculation so that the occurrence of very small or very large numbers is

avoided [21]. The equilibrium phase diagrams for the system with all round periodic boundary conditions have been studied and found in good agreement with the result based on free energy minimization methods [4]. In the current study, the boundary conditions in top and bottom are changed to velocity boundary type. No shear case is actually the shear with zero shear rate. The simulation is performed on 256×64 lattice with initial mass density $\rho = 1.15$, temperature $T = 1.04$ and cooling rate $\dot{T} = -0.01/(10000\ steps)$. The choosing of the initial mass density and the ratio between lattices in *x* and *y* directions are to ensure that flat interface will form during the phase separation. If the volume fraction of one phase is too small then it will form disk shape (sphere in 3D) because of the lowest surface energy. It can be estimated that the quadrilateral shape will have less surface area than that of a disk shape when the droplet radius is large than N_y/π for the current device. The system temperature drops 0.01 after each 10000 time steps. It has been proved that 10000 time steps are more than enough for system to achieve equilibrium.

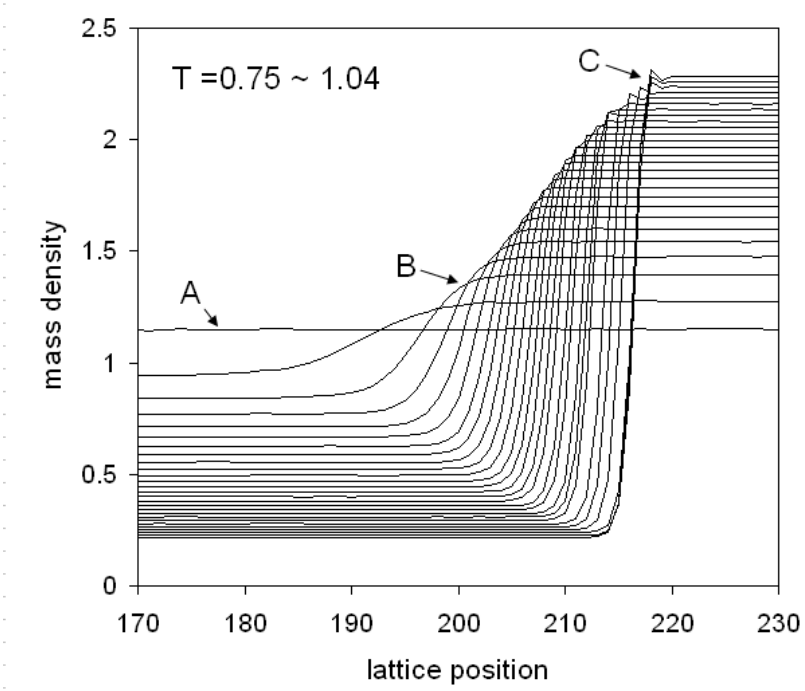


Fig. 2. Mass density distribution profiles across the interface at temperature from 0.75 to 1.04 in 256×64 lattices with $\dot{\gamma} = 0$ and initial uniform mass density $\rho = 1.15$. The label A points to the position where the temperature is above the critical point and no phase separation takes place (T > 1.01). The label B points to the profiles where phase separated but temperature is not very low. The label C points to the profiles where the temperature is low and density difference between two phases are large.

Fig. 2 illustrated the mass density distribution profiles for the van der Waals fluids at zero shear rates. The starting temperature is 1.04 and there is no phase separation observed until the temperature falls below 1.01. The label A in Fig. 2 points to the almost straight lines that correspond to the mass density profile at temperature from 1.04 to 1.01. The fluctuations are due to the noise that introduced during the computations. When the temperature falls down to 1.0, the original evenly mixed fluid separates into two phases:

one with mass density ρ = 0.946117 and another with ρ = 1.26727. The mass density changes smoothly and monotonically from 0.946117 to 1.26727 across the interface. As the reduction of system temperature, the mass density differences between the two separated phases are increasing. The monotonic-changed mass density profiles across the interface area remain until the system temperature is above 0.9, as represented by label B. When the system temperature is below 0.9, however, a bump appears in the mass density profile at interface, as is pointed by label C. It is thought that the bump is due to the numerical reason because the gradients of mass density at those cases are very large due to the large mass density difference and thin interface thickness when T<0.9. However, the equilibrium mass densities in each bulk phases are still in good agreement with analytical results made by free energy minimization [4]. The interface thickness in the current model is not constant for to reproduce correct interfacial energy [4], and the issue has been discussed on a basis of Allan-Chan's theory [25]

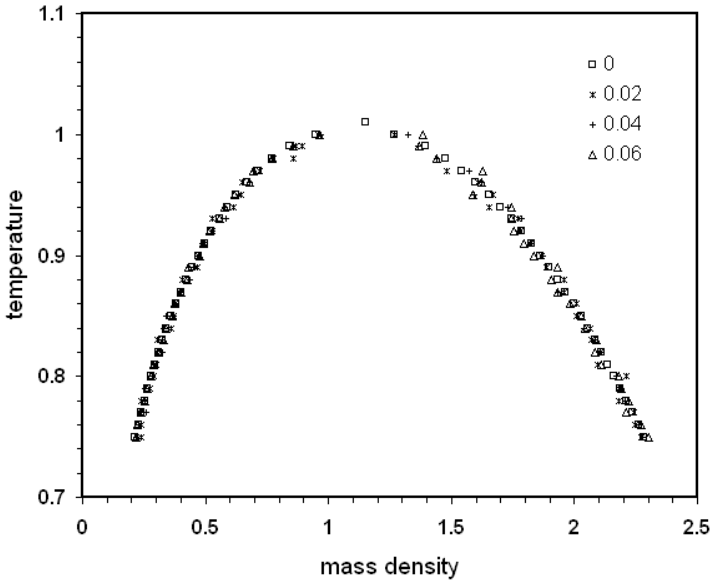
$$\sigma = \varepsilon \int_{-\infty}^{+\infty} \left| \nabla \rho \right|^2 dx \tag{12}$$

where σ is the interfacial energy.

The mass densities at steady state in each phase at different temperatures and shear rates are plotted in Fig. 3(a). The simulation procedure for flow at each shear rate is the same as the early description for Fig. 2. For the non-zero shear rate, lattice *r(i, j)* is initiated with the speed of $\vec{u}(i,\ j) = \left(2vj / N_y - v\right)\hat{x}$. It can be seen that for the boundary shear rates of *v=0.0, 0.02, 0.04* and *0.06* the change of phase equilibrium are very limited. The speed is in a unit of $v_s = \sqrt{3RT/m}$ (for water at 100 °C, it is about 718 m/s) and *v=0.06* is

actually very high. The up limit for speed in LB model is *v=0.1* for the numerical stability consideration. The shear does not make obvious different of equilibrium mass density in bulk phases, especially when the temperature is low and interface energy is large. At the vicinity of critical temperature, large shear causes some obvious derivation but no certain direction of derivation is found.

(a)



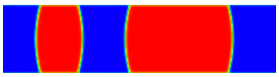
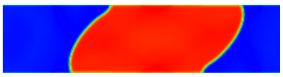
(b)  (c) 

Fig. 3. (a). Equilibrium phase diagram of van der Waals fluid at $v=0.00$, 0.02, 0.04 and 0.06. (b). 2D mass density profile at $v=0.00$. (c) 2D mass density profile at $v=0.02$.

It has been expected that the interface is in planar so that the mass density in separated phases are not affected by curvature of interface. However the speed boundary condition, Eq. (10.1)-Eq.(10.4), applied in the work causes the no-planar interfaces, as illustrated in Fig. 3(b). The mass densities in bulk phases obtained in the current work have been compared with the results with all-round periodic boundary condition simulations in

which planar interface is created and the difference is found negligible small. The reason is that the curvature (1/radius) of the interface in Fig. 3(b) is small. The interface at *v=0.02* is illustrated in Fig. 3(c). The separated phases are deformed by the shear stress.

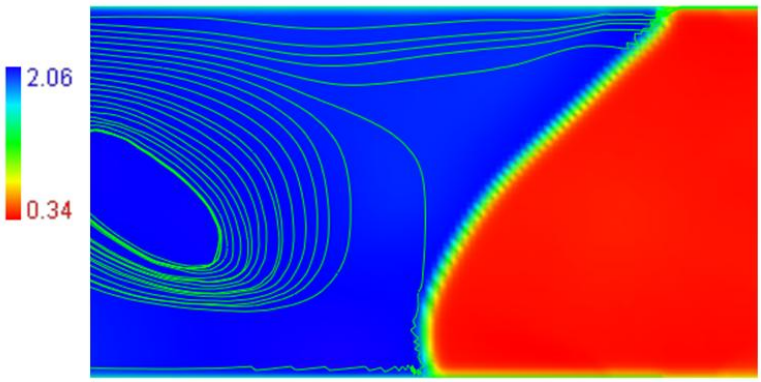


Fig. 4. 32 streamlines in phase separate in shear flow with shear speed of $v = 0.02\hat{x}$. The streamlines are started from lattice position (2, 30+k) (where k=0, 1, … 31) and were computed according to two dimensional nearest neighbor interpolation technique.

For to understand the reason of why the shear flow does not change the equilibrium mass density inside the new phase, the streamlines have been calculated and plotted in Fig. 4 for T=0.85 and $v = 0.02\hat{x}$. Streamline is a path traced out by a massless particle moving with the flow. The two dimensional nearest neighbor interpolation method is used to compute the streamlines and the results are plotted by MatVisual software. The massless particles are initially located at r(2, 30+k) (where k=0, 1, … 31) and move until the they get out of the lattice field. It has been found that no particle can penetrate the interface so that mass density of the new phase is altered in the case. This phenomenon is physically expected. The similar results have been reported in literature [26]. Therefore, the effect of shear on phase thermodynamic properties is very limited when the temperature is low and interface energy is large enough.

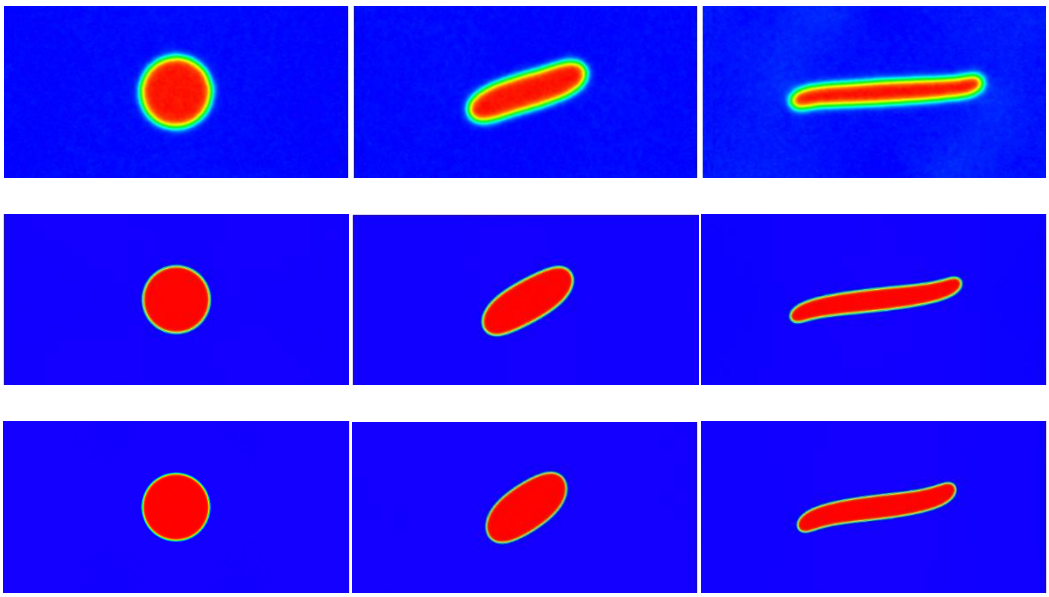


Fig. 5. Equilibrium droplets shape at different temperature and shear rate. From left to right, the temperature is the same but the shear speed is $v = 0.00\hat{x}$, $v = 0.03\hat{x}$ and $v = 0.06\hat{x}$, respectively. Form top to bottom the shear rate is same but the temperature IS $T = 1.00$, $T = 0.94$ and $T = 0.91$.

To understand the effect of shear on equilibrium properties within droplets, Fig. 5 demonstrated the droplets deformation at different temperature and shear rate for a lattice of 512×256. Without shear (or zero shear rate), all droplets are in circular disk shape. The interfacial energies from top to bottom are increasing because of the increasing gradients of mass density. For the same shear rate the droplet with smallest interfacial energy deforms largest. The mass density at the middle cross section inside the droplet at $v = 0.00\hat{x}$, $v = 0.03\hat{x}$ and $v = 0.06\hat{x}$, and $T = 1.00$, $T = 0.94$ and $T = 0.91$ are plotted in Fig. 6. It can be found that the effect of shear rate on the mass density inside the droplets is negligible.

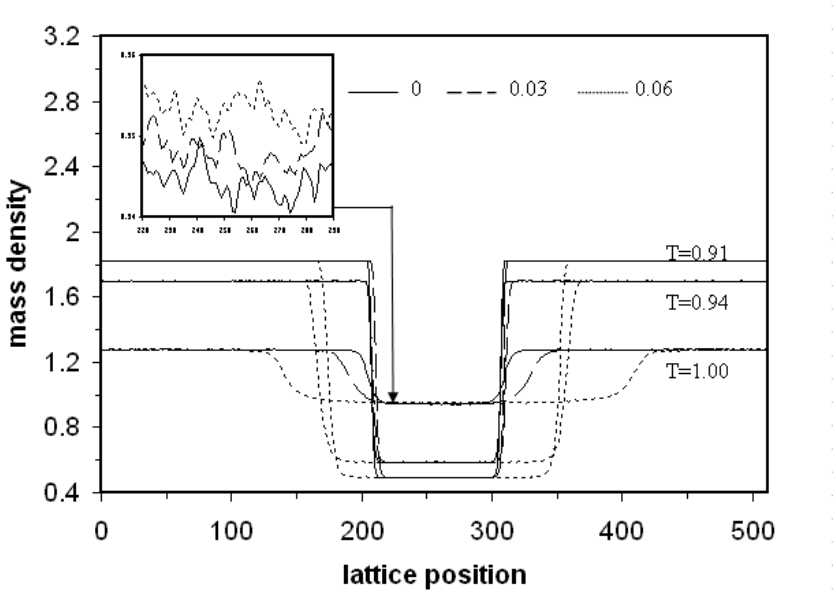


Fig. 6. Mass density distribution profiles for the droplets deformations shown in Fig. 5.

To understand the negligible effect of boundary shear on the mass density inside the droplets, one estimates the shear-induced viscous stress tensor in the droplet. In general, the viscous stress tensor is given by [27]

$$\Gamma = \omega\left(\nabla\vec{v} + \nabla\vec{v}^{T}\right) + \left(\varsigma - \frac{2}{d}\omega\right)\nabla\cdot\vec{v}I \tag{13}$$

where Γ is the viscous stress tensor, ω is shear viscosity, ζ is bulk viscosity, d is dimension and I is a unit matrix. The sup-script T means the transpose of the matrix. In the steady state shear flow, there is only one element, $\partial v_x / \partial y$, in the matrix not to be zero. For a water at 100 °C in a 512×256 lattice with boundary shear velocity $v = 0.06 v_s \hat{x}$, the shear rate is around 2.15×10^{6} s^{-1}, the shear viscosity is around 2.82×10^{-4} Pa·s, and the estimates viscous stress magnitude is $|\Gamma| = 6.06\times10^{2}$ Pa. This is about 0.6% of an atmospheric pressure. Substituting the change of pressure by 0.6% into the state of

equation, Eq. (4), it can be found that the change of the density in the droplet is negligible small.

For the case of $T = 1.00$, the mass density inside the bubble is slightly higher for a higher boundary shear velocity. In a separate simulation using same simulation parameters, the mass density inside the droplet is found increased as the increment of the boundary shear velocity at T=1.0. This phenomenon disappear when T=0.99 and other lower temperature. The results are demonstrated in Fig. 7. The anomalous phenomenon appears only at the temperature near to the critical temperature to phase separation.

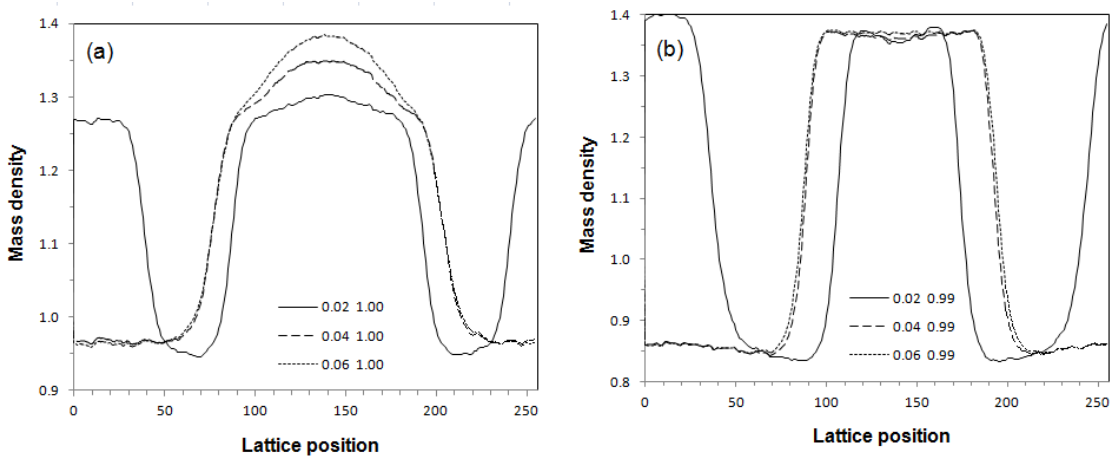


Fig. 7. Shear-induced mass density change inside the droplet at a temperature (a) T=1 and (b) T=0.99.

It has been noticed that the experimental observations of force-induced mixing and shear-induce demixing are in the vicinity of critical temperature. For example the mixing induced by uniform electric fields is detectable only at temperatures that are within a few hundredths of degree or less of the phase transition temperature of the system being

studied [12]. The reason for this is thought to be the weak interfacial energy around the critical temperature so that the flow can penetrate the interface and cause the shift of equilibrium phase diagram. For the temperature well below the critical point, the effect of shear on phase separation is not through the change of phase equilibrium properties. The effect of shear induced droplet break up and down is a different issue.

IV. Conclusions

The major findings of this work are that the phase equilibrium properties of phase separation in shear flow are not obviously affected by the shear rate. The interface prevents mass transport between phases. Droplet deforms under shear stress but the equilibrium properties are not changed. For the phase separations in shear flow that happen at the vicinity of critical temperature much information is unknown.

The mesoscopic interparticle potential is proved an effective way in tackling problems where both thermodynamics and hydrodynamics are equally important. Quantitatively simulation of mesoscopic systems requires expressions of mesoscopic interparticle potentials for those systems.

Acknowledgements

The author is grateful for financial support from the Royal Academy of Engineering, TATA Steel Ltd and EPSRC (EP/L00030X/1) at United Kingdom.

References

[1] L. Kaufman, Calphad **26,** 141(2002).

[2] J. Koplik and J. R. Banavar, Science **257**, 1664(1992).

[3] R.D. Groot and R.B. Warren, J. Chem. Phys. **107**, 4423 (1997).

[4] R.S. Qin, Phys. Rev. E 73, 066703(2006).

[5] E.G. Flekkoy and P.V. Coveney, Phys. Rev. Lett. 83, 1775 (1999).

[6] J.C. Shelley, M.Y. Shelley, R.C. Reeder, S. Bandyopadhyay and M.L. Klein, J. Phys. Chem B 105, 4464 (2001).

[7] A. Onuki, J. Phys. Conden. Matt. 9, 6119 (1997).

[8] J. Schmidt, W. Burchard and W. Richtering, Biomacromolecules 2, 453 (2003).

[9] S. A. Madbouly and T. Ougizawa, Macro. Chem. Phys. 205, 1222 (2004).

[10] E. Helfand and G.H. Fredrickson, Phys. Rev. Lett. 62, 2468 (1989).

[11] S. T. Milner, Phys. Rev. Lett. 66, 1477 (1991).

[12] D. Wirtz and G. G. Fuller, Phys. Rev. Lett. 71, 2236 (1993).

[13] Y. Tsori, F. Tournilhac and L. Leibler, Nature 430 544 (2004).

[14] G.R. McNamara and G. Zenetti, Phys. Rev. Lett. **61**, 2332 (1988).

[15] D. M. Heyes, J. Baxter, U. Tuzun and R.S. Qin, Phil. Trans. R. Sco. Lond. A 362, 1853 (2004).

[16] X.Y. He and L.S. Luo, Phys. Rev. E 55, R6333 (1997).

[17] X.W. Shan and H.D. Chen, Phys. Rev. E **47**, 1815 (1993).

[18] M.R. Swift, W.R. Osborn, and J.M. Yeomans, Phys. Rev. Lett. **75**, 830 (1995).

[19] X.Y. He and G.G. Doolen, J. Stat. Phys. 107, 309 (2002).

[20] J. W. Cahn and J. E. Hilliard, J. Chem. Phys., 31, 688, 1959.

[21] R. S. Qin and H. K. D. B. Bhadeshia, Mater. Sci. Technol., 26, 803 (2010).

[22] M. R. Swift, E. Orlandini, W. R. Osborn and J. M. Yeomans, Phys. Rev. E, 54, 5041 (1996).

[23] X. Y. He and L. S. Luo, J. Stat. Phys. 88, 927 (1997).

[24] Q.S. Zou and X.Y. He, Phys. Fluids 9, 1591 (1997).

[25] S.M. Allen and J.W. Cahn, Acta Metall. 27, 1085 (1979).

[26] X. P. Xu and T. Z. Qian, J. Chem. Phys., 133, 204704 (2010).

[27] P. Espanol and M. Revenga, Phys. Rev E 67, 026705 (2003).